REVISION #1

Solid solution in the fluorapatite - chlorapatite binary system: High-precision crystal structure refinements of synthetic F-Cl apatite

JOHN M. HUGHES[1*], HANNA NEKVASIL[2], GOKCE USTUNISIK[3], DONALD H. LINDSLEY[2], ARON E. CORAOR[2], JOHN VAUGHN[2], BRIAN PHILLIPS[2], FRANCIS M. MCCUBBIN[4], WILLIAM R. WOERNER[2]

[1]Department of Geology, University of Vermont, Burlington, VT 05405, U.S.A.

[2]Department of Geosciences, Stony Brook University, Stony Brook, NY 11794-2100, U.S.A.

3Department of Earth and Planetary Sciences, American Museum of Natural History, New York, NY 10024-5192, U.S.A.

[4]Institute of Meteoritics, Department of Earth and Planetary Sciences, University of New Mexico, Albuquerque, NM 87131, U.S.A.

ABSTRACT

Apatite *sensu lato*, $Ca_{10}(PO_4)_6(F,OH,Cl)_2$, is the tenth most abundant mineral on Earth, and is fundamentally important in geological processes, biological processes, medicine, dentistry, agriculture, environmental remediation, and material science. The steric interactions among anions in the [0,0,*z*] anion column in apatite make it impossible to predict the column anion arrangements in solid solutions among the three end-members. In this work we report the measured atomic arrangements of synthetic apatite in the F-Cl apatite binary with nominal composition $Ca_{10}(PO_4)_6(F_1Cl_1)$, synthesized in vacuum at high temperature in order to minimize both hydroxyl- and oxy-component of the apatite. Four crystals from the high-temperature synthesis batch were prepared to assess the homogeneity of the batch and the precision of the location of small portions of an atom in the apatite anion column by single-crystal X-ray

*Email: jmhughes@uvm.edu

diffraction techniques. Crystals were ground to spheres of ~80 μm diameter, and full-spheres of Mo$K\alpha$ diffraction data were collected to $\theta = 33°$, with average redundancies > 16. Final $R1$ values ranged from 0.0145 to 0.0158; the lattice parameters ranged from $a = 9.5084(2) – 9.5104(3)$, $c = 6.8289(3) – 6.8311(2)$Å. Based on this study, solid solution in $P6_3/m$ apatites along the F-Cl join is attained by creation of an off-mirror fluorine site at (0,0,0.167), a position wherein the fluorine atom relaxes away from its normal position within the {00ℓ} mirror plane in $P6_3/m$ apatites; that relaxation is coupled with relaxation of a chlorine atom at the adjacent mirror plane away from the off-mirror fluorine, allowing acceptable F-Cl distances in the anion column. There are a total of four partially occupied anion positions in the anion column, including two for fluorine [(0,0,1/4) and (0,0,0.167)] and two for chlorine [(0,0,0.086) and (0,0,0)]; the chlorine site at the origin was previously postulated but not observed in calcium apatite solid solutions.

Keywords: Apatite, solid solution, fluorapatite, chlorapatite

INTRODUCTION

Apatite *sensu lato* [$Ca_{10}(PO_4)_6(OH,F,Cl)_2$; OH = hydroxylapatite, F = fluorapatite, Cl = chlorapatite] is the tenth most abundant mineral on Earth and is the most abundant naturally occurring phosphate (Hughes and Rakovan 2002). Apatite forms the foundation of the global phosphorus cycle, and as an ore is the major source of phosphorus. The mineral is critical for production of tremendous quantities of essential fertilizers, detergents and phosphoric acid; the extracted phosphorus is also used in innumerable fundamental applications such as phosphors for lighting and lasing materials, rust removers, coatings for prosthetic devices, motor fuels, and insecticides to name but a few (McConnell 1973). Much more than a source of phosphorus, apatite has many properties that are amenable to its use in a wide range of applications. For example, apatite has been investigated as a solid-state radioactive waste repository, incorporating significant amounts of substituent U and Th (*e.g.*, Ewing and Wang 2002; Rakovan et al. 2005; Luo et al. 2009; Luo et al. 2011; Borkiewicz et al. 2010). It is also employed as a contaminant sequestration agent for *in situ* metal stabilization (*e.g.*, Conca and Wright 1999; Bostick et al. 1999). Additionally, apatite is fundamental in controlling rare-earth and trace element variation in rocks (Hughes et al. 1991), and is the primary mineral used in fission-track determination of rates and dates in geologic processes (Hughes et al. 1990b).

Apatite transcends the inorganic environment, as hydroxylapatite is the main mineral constituent of human bones, teeth, and many pathological calcifications; virtually all structural hard tissue of the human body is formed of apatite materials (an extensive summary is provided in Elliot 2002). Approximately 70% of the U.S. population consumes fluoridated water as an effort to increase the fluorapatite component in their teeth, and the U.S. Centers for Disease Control (1999) lists water fluoridation as one of the ten great public health achievements of the 20th century. Recent research has also demonstrated that apatite composition may be useful in

distinguishing between benign and malignant breast lesions in a non-invasive manner (Kerssens et al. 2010). Apatite is thus unique among minerals in that there is an extensive literature on the phase in the fields of geology, dentistry, medicine, agriculture, biology, and material science (McConnell 1973; Elliott 1994; Kohn et al. 2002), and the importance of studies on the apatite minerals transcends more disciplines than perhaps any other mineral.

The principles of the structure of apatite were determined over 80 years ago (Mehmel 1930; Náray-Szabó 1930). In contrast to more common cation solid solutions in minerals, the solid solution in apatite *sensu lato* is effected by anion substitutions. Because of the large difference in size of the anions, there is a concomitant large structural response to the anion substituents. Hughes et al. (1989) reported the most recent structure refinements on natural near-end-member fluorapatite, chlorapatite, and hydroxylapatite, and commented on the incompatibility of the end-member anion positions in binary and ternary solid solution. Mixing of components with end-member atomic arrangements suggests that binary members of the system must undergo symmetry breaking, possess immiscibility gaps, incorporate essential vacancies with an unknown method of charge balance, and/or possess anion positions that are not currently recognized to effect solid solution. These complications appear particularly likely in apatite along the fluor-chlor binary, and study of those compositions would provide vital clues as to the nature of the accommodation of both halogens in the apatite structure. However, terrestrial apatites are dominated by large hydroxylapatite component abundances; even lunar apatite is not as OH-poor as previously assumed (McCubbin et al. 2010a; Boyce et al. 2010). Synthesis has remained the recognized primary means for obtaining chlor-fluor apatite, yet the difficulty in obtaining low OH abundance and crystals large enough for single crystal x-ray study

has greatly restricted such effort. The work reported here has involved a coupled effort of synthesis and structural study.

SYNTHESIS AND ANALYSIS TECHNIQUES

Apatite Synthesis

Strict stoichiometric control on synthetic apatite requires careful preparation and characterization of starting materials. Starting materials for fluor-chlor apatite synthesis consisted of β tri-calcium phosphate (TCP) and $CaCl_2$ and/or CaF_2. TCP is generally available commercially with a published analysis to indicate purity; nonetheless, to ensure proper calcium to phosphate ratios in the synthetic apatite, a representative aliquot of the batch of TCP used was analyzed by x-ray diffraction. Through Rietveld analysis, it was found to contain 7 mol% calcium pyrophosphate ($Ca_2P_2O_7$). This Ca-deficiency was corrected by adding $CaCO_3$ and then decarbonating before repeat x-ray analysis. X-ray analysis of the corrected material showed 100% TCP, and there was appropriate weight loss for 100% decarbonation.

During the synthesis of F-Cl apatites, great care must be taken to avoid the unintended incorporation of water; even small amounts of (OH) "impurity" in the anion column can effect column reversals and cause symmetry changes. The use of halides in apatite synthesis has posed a significant problem due to their hygroscopic nature, particularly for the chloride, which retains water readily even at high temperatures. Although very high temperature apatite synthesis (1200-1300 ºC) may induce some dehydration, in air such synthesis leads to the formation of several percent oxy-apatite component (Schettler et al. 2011). In order to minimize the abundance of both hydroxyl- and oxy-apatite component in the apatite synthesized, fused pellets of $CaCl_2$, ~1mm in size, from ampoules sealed under argon, were used as a Cl source, but the ampoules were not opened until immediately prior to weighing. Weight gain trials showed that the

relatively low surface area of the pellets dramatically alleviates the severe hydration problems endemic to exposure of $CaCl_2$ to air. In contrast to $CaCl_2$, exploratory investigations showed that although dehydration of powdered CaF_2 is effected at high temperature, F is also lost likely through the reaction: $CaF_2 + H_2O$ (air) → CaO + 2 HF (gas). However, this dehydration is then negated by the CaO produced which rapidly acquires H_2O and CO_2 as it cools in air. Conditions under which CaF_2 can be dried without significant F loss were optimized by powder diffraction studies coupled with heating temperature and drying time trials.

For apatite synthesis, a homogenized "pre-mix" of corrected TCP and dried CaF_2 was made in an amount just sufficient to fill the Pt capsule. Following this, an ampoule of fused anhydrous $Ca(Cl)_2$ pellets was opened quickly and the requisite amount weighed out. The pellets were quickly stirred into the "pre-mix" and the entire mass transferred to the Pt capsule, which had been welded on one end. The Pt capsule, crimped closed but not welded, was placed into a 7 mm ID silica-glass tube. The assembly was then dried under vacuum at ~730°C for 20 minutes, and the silica glass tube sealed while still under vacuum. The evacuated silica glass tube was heated to 1100°C for a period of 21 days. The weighing technique assured that the bulk composition within the Pt capsule was correct, but the $Ca(Cl)_2$ pellets were not uniformly distributed. Based on the TCP-$CaCl_2$ phase diagram (Nacken 1912), it is likely that at 1100°C, mixtures along the fluor-chlorapatite join have a small amount of melt to aid in homogenization and growth of large crystals.

Powder X-ray diffraction of the resulting bulk synthetic material showed only apatite, with a =9.50640(4) and c = 6.82833(3) Å. The synthetic product yielded large apatite single crystals that could be ground to ~80 μm spheres. Four apatite crystals from the reaction products were ground using a Bond sphere grinder; quadruplicate samples were selected to confirm the

homogeneity of the reaction products and assess the precision of the X-ray results. Two of these samples were analyzed by electron microprobe after single crystal study to determine their composition.

Electron Microprobe Analysis

Two of the synthetic apatite grains (HNF5CL5_9 and HNF5CL5_10) were analyzed using the JEOL 8200 electron microprobe in the Institute of Meteoritics at the University of New Mexico using Probe for EPMA^{TM} (PFE) software. An accelerating voltage of 15 kV and a nominal probe current of 20 nA were used during each analysis. We analyzed for the elements Si, Mg, Ca, Na, P, F, and Cl. F was analyzed using a light-element LDE1 detector crystal, and Cl was analyzed using a PET detector crystal. Ca and P were standardized using Durango apatite. F was standardized using strontium fluoride, and Cl was standardized on a sodalite grain. Na was standardized using Amelia albite, Si was standardized using Taylor quartz, and Taylor olivine was used as an Mg standard. We used a 5 μm spot for standardization and analysis of all apatite grains.

Hydroxyl content cannot be measured directly by the EPMA technique; however, a missing component in the X-site of the apatite can be calculated on the basis of stoichiometry. If both F and Cl are analyzed with sufficient accuracy, this missing component can be attributed to some combination of the anions OH^-, O^{2-}, CO_3^{2-}, S^{2-}, Br^-, and I^- and/or structural vacancies (Pan and Fleet 2002) and/or structural H_2O (Mason et al. 2009; Yoder et al. 2012). The most likely missing component in our synthetic system is OH^- or structural vacancies due to the limitations we imposed on the composition of the system during synthesis.

Stormer et al. (1993) documented that fluorine and chlorine X-ray count rates change with time during electron microprobe analysis of apatite as a function of crystallographic orientation. Accordingly, we monitored the synthetic apatite analyses for time-dependent count rates and discovered that our fluorine count rates were not always constant during the course of an analysis. Conversely, chlorine count rates were found to be constant for all of our analyses. To correct for the fluorine X-ray count variations, we used a time-dependent intensity (TDI) correction in the PFE software to monitor the time dependence and then project fluorine X-ray count rates to time-zero following the procedure of McCubbin et al. (2010b; 2011). We report electron microprobe data from two single-crystals that were used in the single-crystal X-ray diffraction analysis (HNF5CL5_9 and HNF5CL5_10).

BSE images of crystals HNF5CL5-9 and HNF5CL5-10 are shown in Figure 1, and electron microprobe data are given in Table 1. Each apatite grain was homogeneous with only very small variations among analyses. However, there were minor amounts of unreacted TCP in discrete clumps. We suspect that this was due to hydration of the $CaCl_2$ during weighing and therefore, a smaller chloride yield per unit weight, incomplete drying of CaF_2, or a combination of both. Table 1 also shows calculated structural formulae (based on 26 anions). These indicate that the composition of individual crystals differed from the target of fluor:chlorapatite ratio of 1:1, varying from 0.94 to 1.04. The small computed H_2O contents suggest that the apatites, as desired, lie very close, if not on, the fluorapatite-chlorapatite join. However, in order to further evaluate the possible presence of OH, $^{31}P\{^1H\}$ CP/MAS and single-pulse (SP) NMR spectra were obtained.

Solid-State Nuclear Magnetic Resonance (NMR)

Solid-state $^{31}P\{^{1}H\}$ CP/MAS and ^{31}P single-pulse (SP) NMR spectra were obtained on a 400 MHz (9.4 T) Varian Inova spectrometer operating at 161.877 MHz for ^{31}P and 399.895 MHz for ^{1}H at a spinning rate of 5 kHz, using a Varian Chemagnetics T3 probe configured for 3.2 mm rotors. The ^{1}H B_1 field was 50 kHz, and cross-polarization was achieved using a linear ramp of the ^{31}P B_1 field of approximately ± 5 kHz, centered near the n = 1 sideband match condition. The contact time was 2 ms with a 2s relaxation delay. Fully relaxed ^{31}P SP spectra were acquired with a 5 μs (90°) pulse and a relaxation delay of 300 s. ^{31}P chemical shifts were measured relative to that of synthetic hydroxylapatite, taken to be +2.65 ppm from 85% H_3PO_4 *(aq)*.

The ^{1}H NMR spectra were obtained on a 500 MHz Varian Infinity Plus spectrometer (499.784 MHz for ^{1}H, 202.318 MHz for ^{31}P) at a spinning rate of 8 kHz, using a Varian T3 5 mm probe configured for low-^{1}H background. ^{1}H resonances from ^{1}H located near ^{31}P were selected by $^{1}H\{^{31}P\}$ REDOR difference spectroscopy (Guillon and Schaefer 1989). A 2 ms dephasing pulse was used, which was sufficient to remove > 95% of the ^{1}H signal in hydroxylapatite. ^{1}H chemical shifts were measured relative to that of synthetic hydroxylapatite, set to +0.2 ppm.

The NMR spectra were obtained from a bulk sample of the synthetic 50-50 fluor-chlorapatite from which the HNF5Cl5_9 and HNF5CL5_10 grains were taken. A single, broad peak (5 ppm FWHM) is observed in the $^{31}P\{^{1}H\}$ CP/MAS spectrum of the bulk 50-50 fluor-chlorapatite at 2.5 ppm, which suggests that the ^{1}H associated with phosphorus is in an apatite-like environment, which gives a chemical shift of 2.65 ppm in the end member hydroxylapatite composition. This result was confirmed by $^{1}H\{^{31}P\}$ REDOR experiments, from which the REDOR difference spectrum features a single resonance at δ_H = 1.6 ppm which can be assigned to OH groups. McCubbin et al. (2008) described a 50-50 fluor-chlorapatite composition whose

^{1}H NMR spectrum features resonances at +6.6, +3.2, +1.9 and +1.1 ppm, the latter two of which were unambiguously assigned to OH groups in mixed apatites due to close correspondence with work by Yesinowski and Eckert (1987). The single ^{1}H resonance at δ_H = 1.6 ppm observed in the 50-50 fluor-chlorapatite composition in this work falls well within the OH-bearing mixed apatite range of +1.1 to +1.9 ppm, which strongly suggests that all the ^{1}H present in this composition is found as OH within the apatite structure.

The hydroxylapatite content of the bulk 50-50 fluor-chlorapatite sample was estimated by comparing the intensity ratio of the single-pulse (SP) ^{31}P and cross-polarization ^{31}P{^{1}H} NMR (CP) spectra with that from a synthetic pure hydroxylapatite under identical acquisition conditions. The transient-normalized integral ratios of these spectra provide the relative amount of phosphorus in the sample which is located within several angstroms of ^{1}H. The CP ^{31}P{^{1}H} to SP ^{31}P integral ratios for crystalline hydroxylapatite and bulk 50-50 fluor-chlorapatite were determined to be 1:8 and 1:1900, respectively. Using these values, the fraction of ^{31}P in the 50-50 fluor-chlorapatite that occur in hydroxylapatite-like local configurations was determined to be 1:238, or approximately 0.4 mol%; a similar result was obtained from measurements at 11.7 T under static (non-spinning) conditions. Importantly, CP/SP integral ratios are independent of sample size and rotor configuration.

X-ray Diffraction

The potential difficulty in locating small fractions of a disordered column anion at various positions in the anion column required unusual care to be taken in the diffraction experiments. The data were collected at STP with a Bruker Apex II CCD single-crystal diffractometer using graphite-monochromated Mo K_α radiation. Crystal data, data collection

information and refinement details are given in Table 2. Redundant data were collected for an approximate sphere of reciprocal space (4,500 frames, 0.20º scan width; average redundancy > 16), and were integrated and corrected for Lorentz and polarization factors, and corrected for absorption, using the Bruker programs Apex2 package of programs. The structures were refined in space group $P6_3/m$ with SHELXL-97 (Sheldrick 2008), using scattering factors for neutral atoms, and full-matrix least-squares on F^2, minimizing the function $\Sigma\, w(F_o^2 - F_c^2)^2$ with no restraints. All atoms were refined with anisotropic temperature factors except the column anions; an extinction coefficient was also refined. In earlier studies (*e.g.*, Hughes et al. 1990a), it was found that the use of anisotropic atomic displacement factors for the column anions brought about unreasonable values of U_{33}, an anisotropy that masked the positions of various anion sites occupied by small fractions of a column anion. The occupancy of the column anions was not constrained. After initial refinements for all four crystals, the largest peak in the difference map was found in the same location, suggesting that it resulted from disorder of the O3 atom. That disorder was successfully modeled in all four structures.

Table 3 lists the atom parameters and equivalent atomic displacement parameters, Table 4 presents selected interatomic distances in the F-Cl structures. Table 5 lists anisotropic displacement parameters and Table 6 lists the observed and calculated structure factors for all four structures. Table 7 gives the CIF files for the structures. Tables 5, 6, and 7 are on deposit, and are available as noted below.[2]

[2] Deposit items AM-13-xxx, AM-13-xx1, AM-13-xx2 for anisotropic displacement parameters (Table 5), observed and calculated structure factors (Table 6a-d), and CIFs (Table 7), respectively. Deposit items are available two ways: for paper copies contact the Business Office of the Mineralogical Society of America (see inside front cover of recent issue) for price information. For an electronic copy visit the MSA web site at http://www.minsocam.org, go to the *American Mineralogist* Contents, find the table of contents for the specific volume/issue wanted, and then click on the deposit link there.

RESULTS AND DISCUSSION

In apatite minerals [$Ca_{10}(PO_4)_6(OH,F,Cl)_2$; OH = hydroxylapatite, F = fluorapatite, Cl = chlorapatite], OH, F, and Cl lie in [0,0,*z*] columns along the [00ℓ] edges of the unit cell. The $P6_3/m$ apatite unit cell has (00ℓ) mirror planes at $z = 1/4$ and 3/4. Within those mirror planes, triangles of Ca2 atoms surround the [0,0,*z*] anion column (Figure 2). There are several factors that affect the positions of the anions in the columns, including the size of the anions, the specific nearest-neighbors in the anion column and the electrostatic repulsions from those neighbors, electrostatic attractions to surrounding cations, particularly Ca2 and substituents in that site, any dissymetrization that may occur, and, in OH-bearing apatites, the hydrogen bonding that occurs between the hydroxyl and adjacent column fluorine atoms and possibly with more distant oxygen atoms of the phosphate groups. Taken together, these factors will yield the position of any individual column anion occupant.

Based on previous studies (Hughes et al. 1989 and references therein) in fluorapatite, the F column anion can be accommodated in the Ca2 triangle within the mirror plane, coplanar with the Ca2 atoms. In hexagonal hydroxylapatite, the hydroxyl is slightly larger, and is thus displaced ~0.35Å above *or* below the plane. At each triangle ($z = 1/4$, 3/4) the three Ca2 atoms will bond to a hydroxyl *either* above or below the mirror in a half-occupied position at (0,0,~0.30) *or* (0,0,~0.20); this results in half of the hydroxyls disordered above the plane and half below, yielding a statistical mirror plane over the crystal as a whole but diminished symmetry locally at each mirror plane (positions are given for the anions associated with the mirror plane at $z = 1/4$, and those at the mirror plane at $z = 3/4$ are related by the [0,0,1/2] translation vector from the 6_3 screw axis). In hexagonal chlorapatite, the much larger Cl atom (F = 1.33Å, Cl = 1.84Å) is similarly displaced above or below the plane, but because of the larger

size of the Cl atom that displacement is ~1.3Å above *or* below the plane, to positions at (0,0,~0.44) or (0,0, ~0.06). As is the case for the hydroxyls in hydroxylapatite, the disordering of Cl atoms with 1/2 of the atoms above the plane and 1/2 below the plane allows retention of $P6_3/m$ symmetry in the crystal as a whole but causes diminished local symmetry at each mirror plane. In both hydroxylapatite and chlorapatite, reversals of the occupants of the anion column occur with incorporation of substituents and/or vacancies; without such incorporation, the column anions are ordered entirely above or entirely below in given columns, leading to $P2_1/b$ symmetry (Hounslow and Chao 1970; Elliot et al. 1973; Hughes et al. 1989; Hughes and Rakovan 2002).

Apatite solid solution occurs with variation in relative abundances of column anions. However, the atomic arrangements of mixtures of the end members of calcium apatite in solid solution are not predictable from the atomic arrangements of the end members (Hughes and Rakovan 2002; Hughes et al. 1989). An example of the response in column anion positions to solid solution is demonstrated in (F, OH, Cl) ternary apatites. Figure 3 depicts the column anion positions in hexagonal ternary apatite, and illustrates the role of an additional Cl site, Cl*b*, not found in end-member chlorapatite (Hughes et al. 1990a). In hexagonal ternary apatite, the Cl*b* position relaxes approximately 0.5 Å closer to its associated mirror plane [to (0,0,~0.37) or (0,0,~0.13) for the mirror plane at $z = 1/4$]. As shown in Figure 2, this allows sufficient distance (2.95Å) for the accommodation of an (OH) anion at the next mirror plane, which, in turn, allows reversal of the anion column and maintenance of $P6_3/m$ symmetry. Thus, in ternary apatite, solution among the end-members is attained by addition of a site that accommodates a chlorine atom in a site not found in the end-member.

The F-Cl binary of the ternary OH-F-Cl apatite system is particularly complex. As noted by Hughes and Rakovan (2002), Hughes et al. (1989), and Mackie and Young (1974), end-member fluorapatite and chlorapatite anion column positions suggest that F and Cl atoms are incompatible in the anion columns (although as little as 12-15% occupancy of the halogen site by hydroxyl will lead to compatibility of F and Cl neighbors in the anion columns; McCubbin et al. 2008). Figure 4 depicts the anion column in fluor-chlorapatite, using anion positions in the fluorapatite and chlorapatite end-members in addition to the Cl*b* site found in ternary apatite. The sequence of anions depicted allows reversal of the sense of the anion positions relative to the mirror plane (above or below), thus preserving $P6_3/m$ symmetry. In addition, the depicted anion sequence yields the greatest distance between fluorine and chlorine anions in the column. It is clear from the unacceptably short F-Cl distance (~2.60Å) that symmetry breaking, the presence of immiscibility gaps, the incorporation of essential vacancies with an unknown method of charge balance, and/or the presence of new anion positions is necessary to effect solid solution along the F-Cl apatite binary based on this analysis using the endmember structures.

The successful synthesis of fluor-chlorapatite in this study has enabled elucidation of the method of solid solution along the binary, and builds upon the earlier work of Mackie and Young (1974). Figure 5 depicts the anion column in the fluor-chlorapatites determined in this study, and the *z* position of each column anion (in a 0,0,*z* position) is given in Table 3. The fluorine atoms in fluorapatite exist within the Ca triangles in the {00ℓ} mirror planes (Fig. 2), at the (0,0,1/4) position. However, because of the interactions with adjacent chlorine atoms, the fluorine atoms in fluor-chlorapatite occupy two positions in the binary anion column. The position at (0,0,1/4), as found in end-member fluorapatite (Hughes et al. 1989), contains a slight majority of the fluorine in these crystals. However, a new, off-mirror fluorine site is also present in the column,

a site that is not found in any natural apatites described to date. That position, at (0,0,~0.167), in which the fluorine is relaxed from the z = 1/4 mirror plane by ~0.57Å, allows a Cl*b* atom nearest-neighbor at the adjacent z = 3/4 mirror plane. The relaxation of the Cl*b* atom *closer* to its associated mirror plane at z = 3/4, and the relaxation of the F*b* atom *farther* from its associated mirror plane at z = 1/4, allows sufficient distance (2.86 Å) for F-Cl neighbors to coexist in the binary anion column.

The Cl atoms in this fluor-chlorapatite exist at positions that are not seen in other calcium apatite compositions. The Cl position in end-member hexagonal chlorapatite is found at (0,0,~0.56), as noted in previous studies, in this case the value for that Cl atom disordered below the plane at z = 3/4. In the F-Cl binary solid solution, the majority of the Cl is found in the position labeled Cl*b*, at a position of (0,0,~0.59) (Table 3). The relaxation of that Cl atom toward its mirror plane, as noted above, allows for a 2.86Å Cl-F distance when coupled with the ~0.57Å shift of the off-mirror fluorine atom.

In a previous attempt at elucidating the method of accommodation of Cl and F in the binary chlor-fluorapatite anion column, Mackie and Young (1974) undertook crystal structure refinements of two different compositions along the binary, with final R values > 4%. Although their results were similar for Cl*b*, F, and F*b* (using the atom nomenclature of this study), in this study we recognize an additional Cl site (labeled Cl*a*) at (0,0,0) that was present in each of the four samples studied. Although Mackie and Young (1974) did not recognize or refine this position in their structure refinement, they did suggest that it may be partially occupied in their discussion of excess halogens. Although that Cl*a* site has the lowest occupancy of the column anion sites (~8% of the total sites), it is indeed "real" as demonstrated by the large difference peak (*ca*. 1.5 e^{-}•$Å^{-3}$) that is found in each of the four structures when the Cl*a* site is removed

337 from the refinement. The presence of the Cl*a* confirms the conjecture by Mackie and Young
338 (1974) of its existence.

339 The column anion sites found in the binary apatite along the F-Cl join differ from those in
340 end-member fluorapatite and chlorapatite in order to accommodate the solution of the two
341 column anions. However, the refined positions must yield reasonable bond distances to the
342 surrounding Ca atoms in the (00ℓ) Ca2 triangle (Fig. 2); those bond distances are listed in Table
343 4. For the bond valence values (*vu*) calculated from those distances (constants from Brese and
344 O'Keeffe 1991), the F and F*b* atoms are underbonded in their column sites (0.66, 0.54 *vu* for F
345 and F*b*, respectively, in all four structures), and the Cl*a* and Cl*b* sites are overbonded (1.26, 1.38
346 *vu* for Cl and Cl*b*, respectively, in all four structures), although it should be noted that the
347 fluorine atoms are also underbonded (0.84 *v.u.*; Hughes et al. 1989) in pure fluorapatite.
348 Although it was not modeled in this study, it may be that there is disorder of the Ca2 atoms in the
349 Ca2 triangle surrounding the anion column. Hughes et al. (1990a) and Sudarsanan and Young
350 (1978) noted and modeled such disorder in their studies, demonstrating that disorder occurred
351 among the Ca2 atoms as a function of the column anion to which they bonded. We can suggest
352 that such disorder undoubtedly takes place in the fluor-chlorapatites studied herein, and the
353 larger value of U_{22} among the anisotropic thermal parameters supports that suggestion.
354

355 **The possibility of excess halogens in the anion column and the Cl site at (0,0,0)**

356 In each unit cell of apatite there are two anions in the anion column, located within (F), or
357 disordered about (Cl, OH), one of the (00ℓ) mirror planes located at $z = 1/4$ and $z = 3/4$. In their
358 analysis of fluor-chlorapatite, Mackie and Young (1974) noted (F + Cl) > 2 halogen atoms per
359 formula unit (*apfu*) for their two samples, both by chemical analysis (2.06, 2.25 halogen *apfu* for

two samples) and by X-ray site refinement (2.09, 2.19 *apfu*). In the samples described herein, an excess of halogens was also noted by X-ray site refinement, with an average of 2.22 halogens/unit cell. However, this halogen excess was not supported by the results of the chemical analysis of the apatites by electron microprobe. We believe that the microprobe analyses, with their coincidence with the stoichiometry of the reactants, are correct in demonstrating that there are no excess halogens in the F-Cl anion column of our samples. However, the reasoning of Mackie and Young (1974) in explanation of the excess halogens provides an explanation of the Cl site at (0,0,0), which they suggested exists but was not found in their structure study; as noted previously, the evidence for Cl occupancy at that site in the present work is unassailable.

The presence of a Cl site (Cl*a*) at (0,0,0) presents steric constraints in interactions with other anions in the anion column. The greatest distance for the short contact between the Cl*a* atom and its anion column neighbor would be 2.83Å, the distance to a neighboring Cl*b* atom, considered too close for a Cl-Cl interaction, but ideal for a Cl-F interaction.

In their deduction of anion positions in the column, Mackie and Young suggested three criteria, slightly modified here: 1) the interatomic distances between occupants of the anion column must be of reasonable length, 2) the anions must occupy positions found in the structure refinement, and 3) F can occupy a Cl site but Cl cannot occupy an F site because of the resulting short Ca-Cl distances. It is this third criterion that demonstrates how the Cl site at (0,0,0) can exist.

Figure 6 depicts an anion sequence in which one Cl*b* site (that at $z = 0.587$) is occupied by a fluorine anion. In that sequence, the presence of that F anion allows sufficient distance between that anion and an adjacent Cl*a* anion at (0,0,0). Relatively few of the Cl positions are of type Cl*a* (*ca*. 8%), but, as predicted by Mackie and Young (1974), they do exist. The presence of

these sites is effected by a column F anion occupying a Cl site, yielding an ideal F-Cl distance in the anion column.

IMPLICATIONS

Apatite is one of the most common minerals on Earth, and is fundamentally important in geological processes, biological processes, medicine, dentistry, agriculture, environmental remediation, and material science. Despite the widespread interest in the phase and the dependence of all properties on the arrangement of atoms, the atomic arrangements of the members of the binary and ternary system are not well understood, as they are not predictable from the structures of the end-members because of steric interactions between and among the (F,OH,Cl) occupants along the [0,0,*z*] anion column. This work demonstrates how solid solution is attained in apatite compositions along the F-Cl binary. We are continuing to synthesize and characterize members of the apatite ternary system, and further elucidate the steric interactions between and among the occupants of the anion column.

ACKNOWLEDGEMENTS

Support for this work was provided by the National Science Foundation through grant EAR-1249459 to JMH and HN and EAR-809283 to HN. FMM acknowledges support from the NASA Mars Fundamental Research Program during this study (NNX13AG44G), and WRW acknowledges financial support provided by the National Science Foundation (NSF) through Collaborative Research in Chemistry (CHE0714183). The manuscript was improved by reviews by John Rakovan and Claude Yoder, for which we are very appreciative.

REFERENCES CITED

Borkiewicz, O.J., Rakovan, J., and Cahill, C.L. (2010) In situ time-resolved studies of apatite formation pathways. American Mineralogist, 95, 1224-1236.

Bostick, W. D., Jarabek, R.A., Bostick, D.A., and Conca, J. (1999) Phosphate-induced metal stabilization: Use of apatite and bone char for the removal of soluble radionuclides in authentic and simulated DOE groundwaters. Advances in Environmental Research, 3, 488-498.

Boyce, J. W., Liu Y., Rossman, G. R., Guan, Y., Eiler, J. M., Stolper, E. M., and Taylor, L. A. (2010) Lunar apatite with terrestrial volatile abundances. Nature Letters, 466, 466-469.

Brese, N.E., and O'Keeffe, M. (1991) Bond-valence parameters for solids. Acta Crystallographica, B47, 192-197.

Centers for Disease Control and Prevention (1999) Ten great public health achievements--United States, 1900-1999. Morbidity and Mortality Weekly Report, 48(12), 241-243.

Conca, J., and Wright, J. (1999) "PIMS™: A Simple Technology for Clean-Up of Heavy Metals and Radionuclides Throughout the World," In *Environmental Challenges of Nuclear Disarmament, The Proceedings of the NATO Advanced Research Workshop*, T.E. Baca, ed., Krakow, Poland, November 8-13,1998, p. 1-13.

Elliot, J.C., Mackie, P.E., and Young, R.A. (1973) Monoclinic hydroxylapatite. Science, 180, 1055-1057.

Elliott, J. C. (1994) Structure and chemistry of the apatites and other calcium orthophosphates. Elsevier, Amsterdam, 389 pp.

Elliot, J.C. (2002) Calcium Phosphate Biominerals. *In* Kohn, M., J.F. Rakovan and J.M. Hughes, Eds. (2002) *Phosphates: Geochemical, Geobiological and Materials Importance,* 427-

454. Mineralogical Society of America Reviews in Mineralogy and Geochemistry Series, Vol. 48.

Ewing, R.C., and Wang, L.M. (2002) Phosphates as Nuclear Waste Forms. *In* Kohn, M., J.F. Rakovan & J.M. Hughes, Eds. (2002) *Phosphates: Geochemical, Geobiological and Materials Importance,* 673-699. Mineralogical Society of America Reviews in Mineralogy and Geochemistry Series, Vol. 48.

Guillon, T., and Schaefer, J. (1989) Rotational-echo double-resonance NMR. Journal of Magnetic Resonance, 81, 196–200.

Hounslow, A.W., and Chao, G.Y. (1970) Monoclinic chlorapatite from Ontario. Canadian Mineralogist, 10, 252-259.

Hughes, J.M., Cameron, M. and Crowley, K.D. (1989) Structural variations in natural F, OH and Cl apatites. American Mineralogist, 74, 870-876.

Hughes, J.M., Cameron, M. and Crowley, K.D. (1990a) Crystal structures of natural ternary apatites: solid solution in the $Ca_5(PO_4)_3X$ (X = F, OH, Cl) system. American Mineralogist, 75, 295-304.

Hughes, J.M., Cameron, M. and Crowley, K.D. (1990b) Annealing of etchable fission-track damage in F-, OH-, Cl- and Sr-apatite: 2. Correlations with crystal structure. Nuclear Tracks and Radiation Measurements, 17(3), 417-418.

Hughes, J. M., Cameron, M. and Mariano, A.N. (1991) Rare-earth element ordering and structural variations in natural rare-earth-bearing apatites. American Mineralogist, 76, 1165-1173.

Hughes, J.M. and Rakovan, J. (2002) The Crystal Structure of Apatite, $Ca_5(PO_4)_3(F,OH,Cl)$. *In* Kohn, M., J.F. Rakovan & J.M. Hughes, Eds. (2002) *Phosphates: Geochemical,*

Geobiological and Materials Importance, 1-12. Mineralogical Society of America Reviews in Mineralogy and Geochemistry Series, Vol. 48.

Kerssens, M.M., Matousek, P., Rogers, K., and Stone, N. (2010) Towards a safe non-invasive method for evaluating the carbonate substitution levels of hydroxyapatite (HAP) in microcalcifications found in human breast tissue. Analyst, 135(12), 3156-3161.

Kohn, M., Rakovan, J. and Hughes, J.M., Eds. (2002) *Phosphates: Geochemical, Geobiological and Materials Importance*. Reviews in Mineralogy and Geochemistry Series, Volume 48. Mineralogical Society of America, Washington, DC, 742 + xvi pp.

Luo, Y., Hughes, J.M., Rakovan, J., and Pan, Y. (2009) Site preference of U and Th in Cl, F, Sr apatites. American Mineralogist, 94, 345-351.

Luo, Y., Rakovan, J. Tang, Y., Lupulescu, M., Hughes, J.M., and Pan, Y. (2011) Crystal chemistry of Th in fluorapatite. American Mineralogist, 96, 23-33.

Mackie, P. E., and Young, R. A. (1974) Fluorine-chlorine interaction in fluor-chlorapatite. Journal of Solid State Chemistry, 11, 319-329.

Mason, H.E., McCubbin, F.M., Smirnov, A., and Phillips, B.L. (2009) Solid-state NMR and IR spectroscopic investigation of the role of structural water and F in carbonate-rich fluorapatite. American Mineralogist, 94(4), 507-516.

McConnell, D. (1973) Apatite: its crystal chemistry, mineralogy, utilization, and geologic and biologic occurrences. Springer-Verlag, New York.

McCubbin, F.M., Mason, H.E., Park, H., Phillips, B.L., Parise, J.B., Nekvasil, H., and Lindsley, D.H. (2008) Synthesis and characterization of low-OH- fluor-chlorapatite: A single crystal XRD and NMR spectroscopic study. American Mineralogist, 93(1), 210-216.

McCubbin, F. M., Steele, A., Hauri, E. H., Nekvasil, H., Yamashita, S., and Hemley, R .J. (2010a) Nominally hydrous magmatism on the Moon. Proceedings of the National Academy of Science, 107, No 25, 11223-11228.

McCubbin, F. M., Jolliff, B. L., Nekvasil, H., Carpenter, P. K., Steele, A., Zeigler, R. A., and Lindsley, D. H. (2011) Fluorine and chlorine abundances in lunar apatite: Implications for heterogeneous distributions of magmatic volatiles in the lunar interior. Geochimica et Cosmochimica Acta, 75, 5073-5093.

McCubbin, F.M., Steele, A., Nekvasil, H., Schnieders, A., Rose, T., Fries, M., Carpenter, P.K., and Jolliff, B.L. (2010b) Detection of structurally bound hydroxyl in fluorapatite from Apollo mare basalt 15058,128 using TOF-SIMS. American Mineralogist, 95(8-9), 1141-1150.

Mehmel, M. (1930) Über die struktur des apatits. Zeitschrift für Kristallographie, 75, 323-331.

Nacken, R. (1912) *In* Phase Diagrams for Ceramists. (Levin, Robbins, McGurddle, Eds.) V2, 1965 Supplement Figure 3800, p. 550.

Náray-Szabó, S. (1930) The structure of apatite $(CaF)Ca_4(PO_4)_3$. Zeitschrift für Kristallographie, 75, 387-398.

Pan, Y.M., and Fleet, M.E. (2002) Compositions of the apatite-group minerals: Substitution mechanisms and controlling factors. Phosphates: Geochemical, Geobiological, and Materials Importance, 48, p. 13-49.

Rakovan, J., Luo, Y., Elzinga, E. J., Pan, Y., Lupulescu, M., and Hughes, J. M. (2005) Structural state of Th in fluoroapatite determined by single crystal XRD and EXAFS. Goldschmidt Conference, Moscow, Idaho, 2005.

Sheldrick, G.M. (2008) A short history of *SHELX*. Acta Crystallographica, A64, 112–122.

Schettler, G., Gottschalk, M. and Harlov, D. (2011) A new semi-micro wet chemical method for apatite analysis and its application to the crystal chemistry of fluorapatite-chlor apatite solid solutions. American Mineralogist, 96, 138-152.

Stormer, J.C., Pierson, M.L., and Tacker, R.C. (1993) Variation of F-X-ray and Cl-X-ray intensity due to anisotropic diffusion in apatite during electron-microprobe analysis. American Mineralogist, 78(5-6), 641-648.

Sudarsanan, K., and Young, R.A. (1978) Structural interactions of F, Cl, and OH in apatites. Acta Crystallographica, B34, 140l-1407.

Yesinowski, J.P. and Eckert, H. (1987) Hydrogen environments in calcium phosphates: ^{1}H MAS NMR at high spinning speeds. Journal of the American Chemical Society, 109, 6274-6282.

Yoder, C.H., Pasteris, J.D., Worcester, K.N., and Schermerhorn, D.V. (2012) Structural water in carbonated hydroxylapatite and fluorapatite: confirmation by solid state 2H NMR. Calcified Tissue International, 2012, 90, 60-67.

514

TABLE 1: Average electron microprobe analyses for two samples of synthetic fluor-chlorapatites.

Oxide	HNF5Cl5-9 (n=10)	HNF5Cl5-10 (n=6)
SiO_2	0.1(3)	0.01(2)
MgO	0.57(3)	0.58(2)
CaO	54.5(4)	54.4(1)
Na_2O	0.07(2)	0.08(1)
P_2O_5	42.0(5)	42.0(2)
F	1.8(2)	1.9(1)
Cl	3.47(5)	3.41(4)
H_2O*	0.06(9)	0.00(5)
-O = F + Cl	1.53	1.58
Total	**101.04**	**100.80**

Structural formulae based on 26 Anions

Mg	0.14	0.14
Ca	9.84	9.84
Na	0.02	0.02
∑Ca-site	**10.00**	**10.00**
Si	0.02	0.00
P	6.00	6.00
∑T-site	**6.01**	**6.00**
F	0.94	1.02
Cl	1.00	0.98
OH*	0.06	0.00
∑X-site	**2.00**	**2.00**

*Calculated by difference assuming F + OH + Cl = 1*apfu*.

Parenthetical numbers represent uncertainty in last reported digit.

515

516 **TABLE 2.** Crystal data and details of structure refinement for synthetic $fluor_{50}chlor_{50}$ apatite

517 crystals.

Sample	HNF5CL5	HNF5CL5-8	HNF5CL5-9	HNF5CL5-10
a(Å)	9.5104(3)	9.5101(2)	9.5100(4)	9.5084(2)
c(Å)	6.8311(2)	6.8300(1)	6.8289(3)	6.8293(1)
V(Å^3)	535.08(3)	534.96(2)	534.86(4)	534.566(18)
θ range(º)	2.47 to 32.90	2.47 to 33.09	2.47 to 32.90	2.47 – 33.09
h,k indices	$-14 \le h,k \le 14$	$-14 \le h,k \le 14$	$-14 \le h,k \le 14$	$-14 \le h,k \le 14$
ℓ indices	$-10 \le \ell \le 10$	$-10 \le \ell \le 10$	$-10 \le \ell \le 10$	$-10 \le \ell \le 10$
Reflections	11,786	11,758	11,787	11,772
Unique reflections	716	717	719	714
% coverage	99.0	98.9	99.4	98.5
Avg. redundancy	16.461	16.399	16.394	16.487
$R_{int.}$	0.0142	0.0189	0.0136	0.0129
Data/Parameters	716/53	717/52	719/52	713/52
GOOF (F^2)	1.143	1.128	1.152	1.153
*R*1, $I > 2\sigma(I)$	0.0152	0.0142	0.0156	0.0153
*wR*2*, $I > 2\sigma(I)$	0.0428	0.0369	0.0434	0.0420
*R*1, all data	0.0158	0.0145	0.0157	0.0154
*wR*2*, all data	0.0431	0.0371	0.0434	0.0420
Largest (+) peak	0.409	0.326	0.0437	0.473 e/Å^3
Largest (-) peak	0.576	0.591	0.610	0.574 e/Å^3

519 *Weighting scheme: $w = 1/[\sigma^2(F_o^2)+(0.0198P)^2+0.3109P]$ where $P = (F_o^2+2F_c^2)/3$.
520

521

522 **Table 3.** Atomic coordinates and equivalent isotropic atomic displacement parameters ($Å^2$) for

523 $fluor_{50}chlor_{50}$ apatite crystals.

524

Sample	atom	x/a	y/b	z/c	U(eq)	Occ.
HNF5CL5	Ca1	2/3	1/3	0.99782(5)	0.01209(9)	$Ca_{1.00}$
HNF5CL5-8		2/3	1/3	0.99782(5)	0.01339(8)	$Ca_{1.00}$
HNF5CL5-9		2/3	1/3	0.99782(5)	0.01214(9)	$Ca_{1.00}$
HNF5CL5-10		2/3	1/3	0.99782(5)	0.01217(9)	$Ca_{1.00}$
HNF5CL5	Ca2	0.00354(3)	0.25496(4)	1/4	0.01637(9)	$Ca_{1.00}$
HNF5CL5-8		0.00352(3)	0.25495(4)	1/4	0.01767(8)	$Ca_{1.00}$
HNF5CL5-9		0.00350(3)	0.25496(4)	1/4	0.01638(9)	$Ca_{1.00}$
HNF5CL5-10		0.00349(3)	0.25495(4)	1/4	0.01644(9)	$Ca_{1.00}$
HNF5CL5	P	0.96903(4)	0.59805(4)	1/4	0.00844(8)	$P_{1.00}$
HNF5CL5-8		0.96900(4)	0.59803(4)	1/4	0.00975(8)	$P_{1.00}$
HNF5CL5-9		0.96902(4)	0.59804(4)	1/4	0.00846(9)	$P_{1.00}$
HNF5CL5-10		0.96902(4)	0.59804(4)	1/4	0.00849(8)	$P_{1.00}$
HNF5CL5	O1	0.15329(12)	0.66594(13)	1/4	0.01403(19)	$O_{1.00}$
HNF5CL5-8		0.15326(11)	0.66591(13)	1/4	0.01538(18)	$O_{1.00}$
HNF5CL5-9C		0.15326(12)	0.66587(14)	1/4	0.01408(19)	$O_{1.00}$
HNF5CL5-10		0.15333(12)	0.66592(13)	1/4	0.01409(18)	$O_{1.00}$
HNF5CL5	O2	0.87623(13)	0.41095(13)	1/4	0.0179(2)	$O_{1.00}$
HNF5CL5-8		0.87623(13)	0.41101(12)	1/4	0.0192(2)	$O_{1.00}$
HNF5CL5-9		0.87618(13)	0.41098(13)	1/4	0.0180(2)	$O_{1.00}$
HNF5CL5-10		0.87619(13)	0.41100(13)	1/4	0.0180(2)	$O_{1.00}$
HNF5CL5	O3	0.9080(8)	0.6442(11)	0.0630(9)	0.0164(7)	$O_{0.70(3)}$
HNF5CL5-8		0.9070(8)	0.6425(10)	0.0629(9)	0.0169(7)	$O_{0.66(2)}$
HNF5CL5-9		0.9080(8)	0.6440(10)	0.0630(9)	0.0162(7)	$O_{0.70(3)}$
HNF5CL5-10		0.9079(8)	0.6441(10)	0.0629(9)	0.0163(7)	$O_{0.70(3)}$
HNF5CL5	O3'	0.9300(12)	0.6745(13)	0.0851(16)	0.0164(7)	$O_{0.30}$
HNF5CL5-8B		0.9293(11)	0.6745(11)	0.0823(15)	0.0169(7)	$O_{0.34}$
HNF5CL5-9		0.9302(12)	0.6752(13)	0.0849(15)	0.0162(7)	$O_{0.30}$
HNF5CL5-10		0.9300(12)	0.6746(13)	0.0852(15)	0.0163(7)	$O_{0.30}$

Sample	atom	x/a	y/b	z/c	U(eq)	Occ.
HNF5CL5	F	0	0	1/4	0.0132(13)	$F_{0.40(1)}$
HNF5CL5-8		0	0	1/4	0.0150(12)	$F_{0.41(1)}$
HNF5CL5-9		0	0	1/4	0.0134(13)	$F_{0.40(1)}$
HNF5CL5-10		0	0	1/4	0.0127(13)	$F_{0.40(1)}$
HNF5CL5	F*b*	0	0	0.1670(15)	0.0059(17)	$F_{0.37(2)}$
HNF5CL5-8		0	0	0.1678(14)	0.0060(17)	$F_{0.36(2)}$
HNF5CL5-9		0	0	0.1668(14)	0.0049(17)	$F_{0.36(2)}$
HNF5CL5-10		0	0	0.1671(14)	0.0054(17)	$F_{0.37(2)}$
HNF5CL5	Cl*a*	0	0	0	0.021(3)	$Cl_{0.08(1)}$
HNF5CL5-8		0	0	0	0.025(3)	$Cl_{0.08(1)}$
HNF5CL5-9		0	0	0	0.020(3)	$Cl_{0.08(1)}$
HNF5CL5-10		0	0	0	0.019(3)	$Cl_{0.08(1)}$
HNF5CL5	Cl*b*	0	0	0.0859(9)	0.0116(12)	$Cl_{0.25(1)}$
HNF5CL5-8		0	0	0.0865(8)	0.0139(11)	$Cl_{0.26(1)}$
HNF5CL5-9		0	0	0.0856(8)	0.0121(11)	$Cl_{0.26(1)}$
HNF5CL5-10		0	0	0.0854(8)	0.0123(11)	$Cl_{0.26(1)}$

525

526

TABLE 4. Selected interatomic distances in fluor-chlorapatites.

	HNF5CL5	HNF5CL5-8	HNF5CL5-9	HNF5CL5-10
Ca1-				
*O1 (x3)	2.4054(7)	2.4053(7)	2.4049(7)	2.4045(7)
*O2 (x3)	2.4522(8)	2.4519(8)	2.4514(8)	2.4513(8)
*O3 (x3)	2.7245(97)	2.7102(87)	2.7229(92)	2.7226(93)
[O3' (x3)]	3.005 (11)	2.9994(84)	3.009(10)	3.005(11)
*Mean	2.527	2.522	2.526	2.526
Ca2-				
O1	2.796(1)	2.796(1)	2.797(1)	2.796(1)
O2	2.337(1)	2.338(1)	2.338(1)	2.337(1)
O3 (x2)	2.322(4)	2.327(5)	2.322(4)	2.321(4)
O3a (x2)	2.561(5)	2.565(6)	2.561(5)	2.561(5)
[O3' (x2)]	2.380(11)	2.362(10)	2.377(10)	2.380(11)
[O3'a (x2)]	2.470(11)	2.473(10)	2.467(10)	2.468(11)
F	2.4081(3)	2.4080(3)	2.4082(3)	2.4077(3)
F*b*	2.474(2)	2.473(2)	2.474(2)	2.473(2)
Cl	2.9522(3)	2.9519(3)	2.9520(3)	2.9516(3)
Cl*b*	2.656(3)	2.654(2)	2.657(2)	2.657(2)
P-				
*O1	1.535(1)	1.535(1)	1.535(1)	1.535(1)
*O2	1.541(1)	1.540(1)	1.541(1)	1.540(1)
*O3 (x2)	1.555(5)	1.552(5)	1.553(5)	1.555(5)
[O3']	1.485(10)	1.503(10)	1.489(10)	1.485(10)
*Mean	1.547	1.545	1.546	1.546

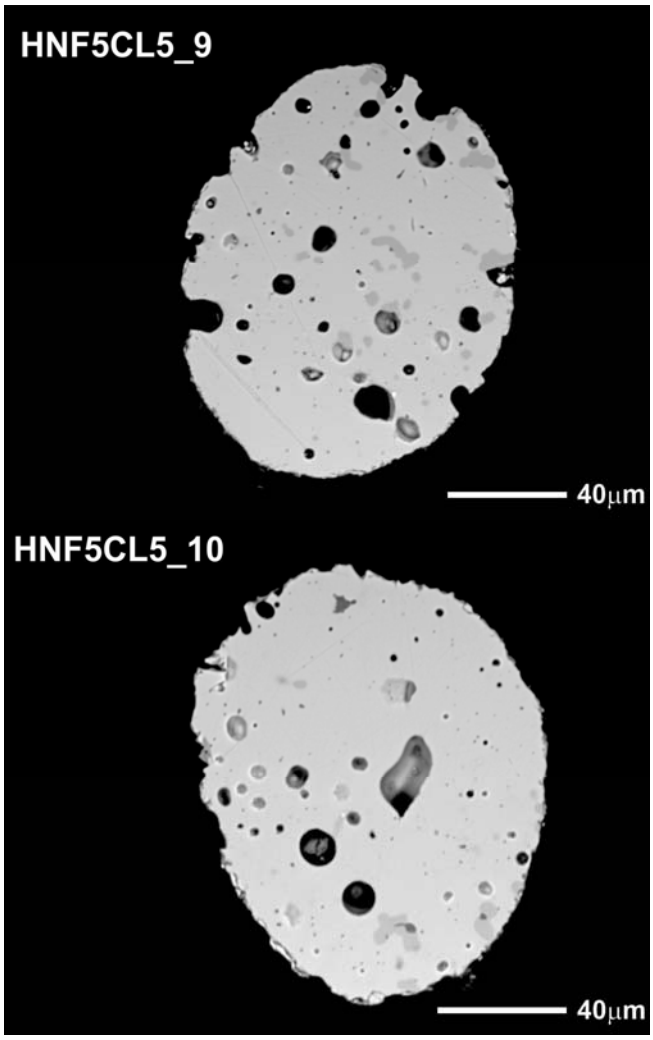

FIGURE 1. Back-scattered electron images of spherically ground apatite single-crystals used in this study and analyzed by EPMA. The black circular features within the grains represent voids within the grains, the irregularly-shaped dark grey patches are minor amounts of unreacted β tri-calcium phosphate, and the bright grey portions that dominate the grain area are apatite.

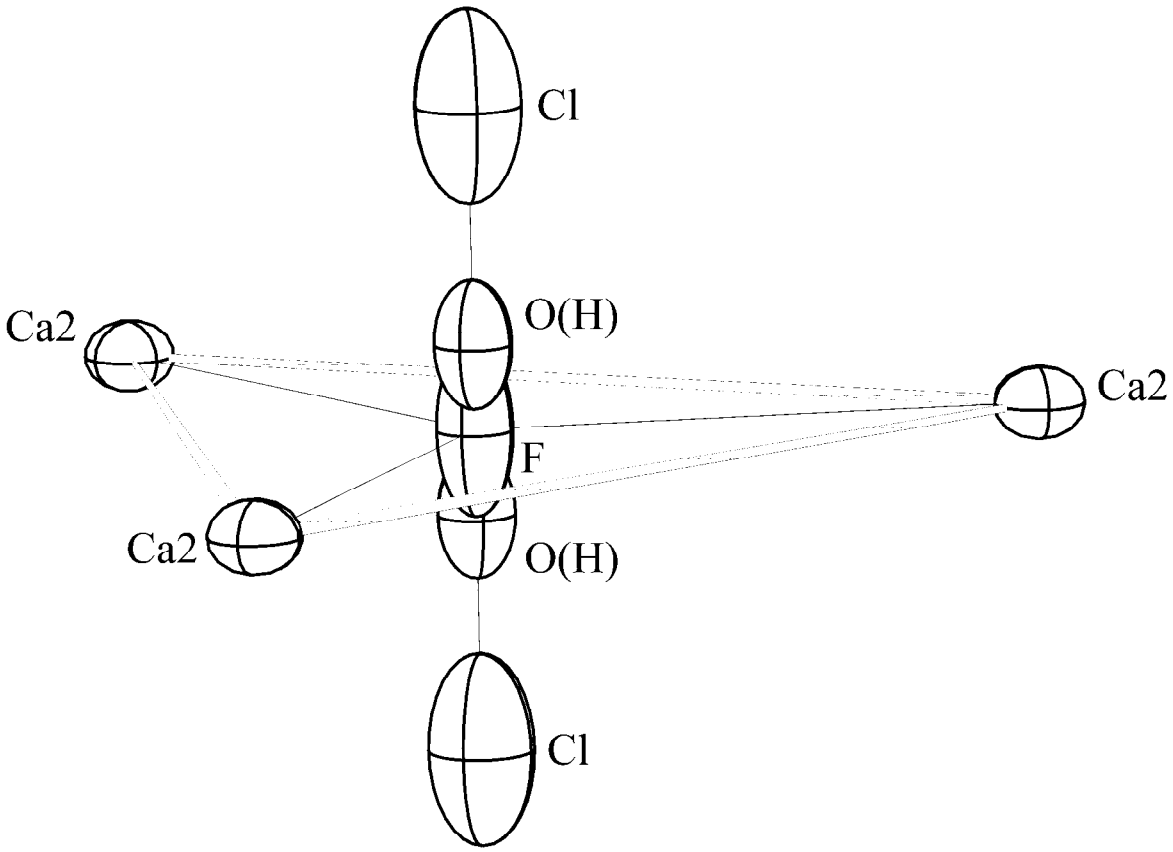

567

568

569 **FIGURE 2**. Apatite column anion positions associated with mirror plane at z = 1/4,
570 displaying column anion positions derived from end-member atomic arrangements. Triangle
571 formed by Ca2 atoms and F atom forms the z = 1/4, 3/4 mirror planes; vertical line is [0,0,z]
572 anion column.

573

574

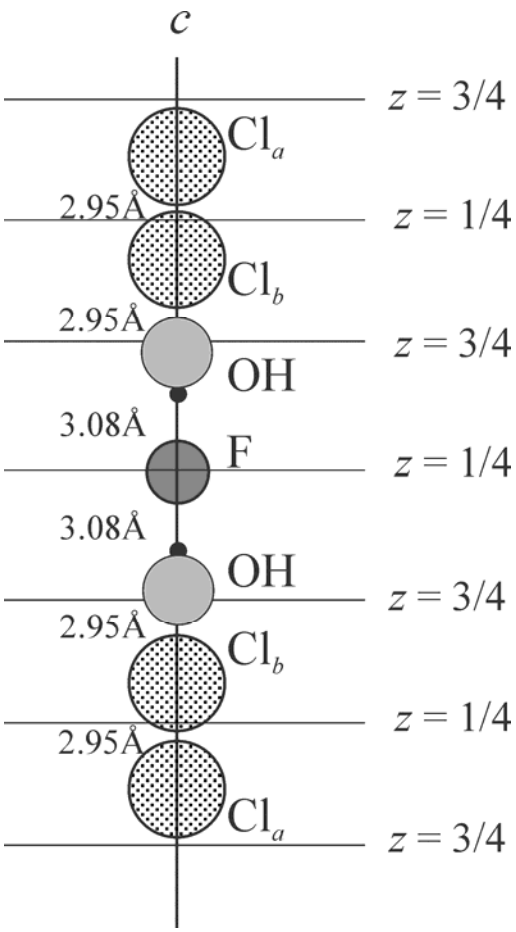

575
576
577

578 **FIGURE 3**. Column anions associated with mirror planes in hexagonal ternary apatite, as
579 discussed in text. A second Cl site, Cl*b*, not found in end-member chorapatite, relaxes towards its
580 associated mirror plane and allows an adjacent (OH) at a permissable distance at the adjacent
581 mirror plane.

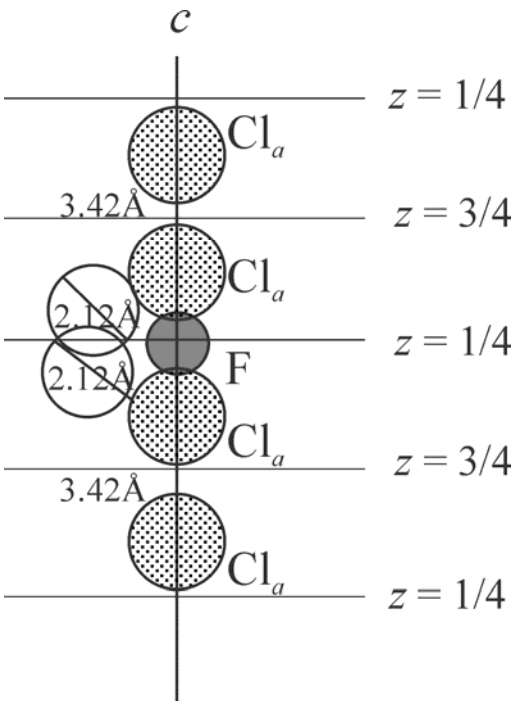

582

583

584

585

586 **Figure 4**. Depiction of anion column in fluor-chlorapatite with anion positions derived from

587 positions in end-member fluorapatite and chlorapatite. Anions are placed so as to yield the

588 greatest distance between Cl and F atoms and allow reversal of the anion column to retain $P6_3/m$

589 symmetry; the Cl-F distance is an impossibly short 2.12Å.

590

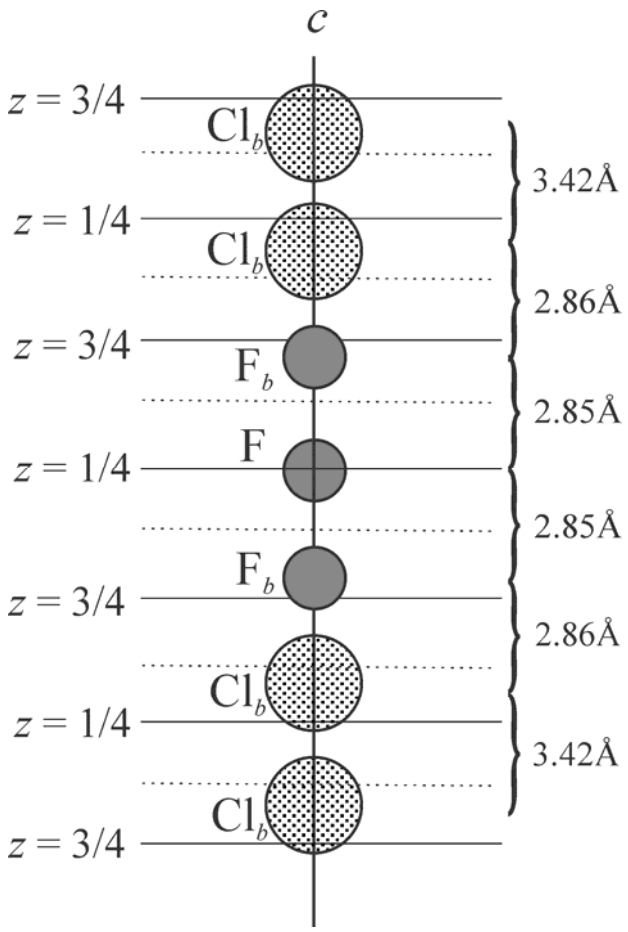

591

592

593 **Figure 5**. Depiction of anion column in fluor-chlorapatite with anion positions derived
594 from diffraction experiments in this study. Dashed lines represent planes at z = 0, 1/2. See Table
595 3 for z coordinates of each (0,0,z) atomic position. Each Fb anion relaxes ~0.55Å from its
596 associated mirror plane, allowing an adjacent Cl*b* atom in the anion column.

597

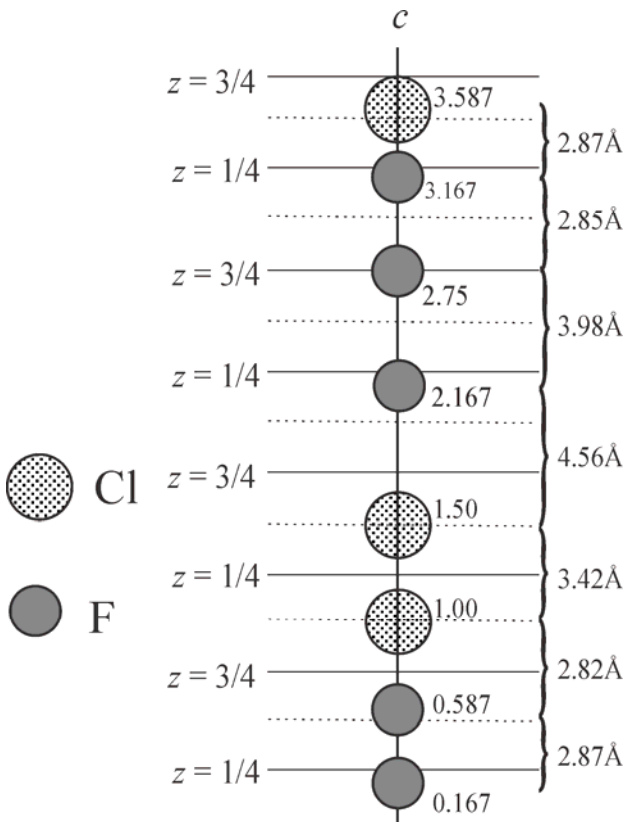

598
599
600
601 **Figure 6**. Depiction of accommodation of Cl*a* atoms at the (0,0,0) position (explanation
602 in text), showing inter-anion distances in the anion column. Fluorine anion at 0.587 occupies a
603 Cl*b* site, allowing the adjacent Cl*a* atom. Numbers to the right of each atom are the *z* coordinate
604 of each of the anions in their (0,0,*z*) position.

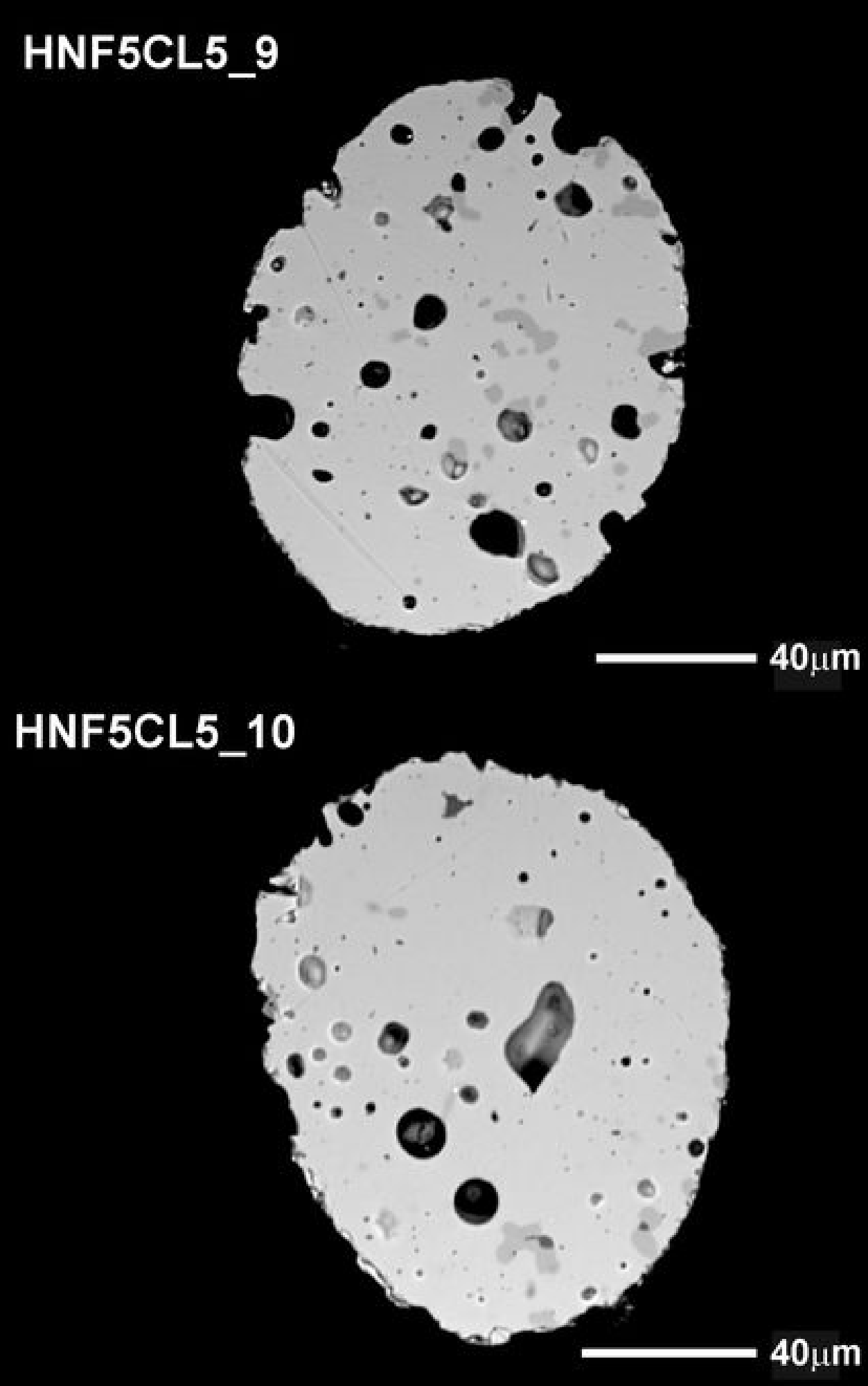
HNF5CL5_9
40μm
HNF5CL5_10
40μm

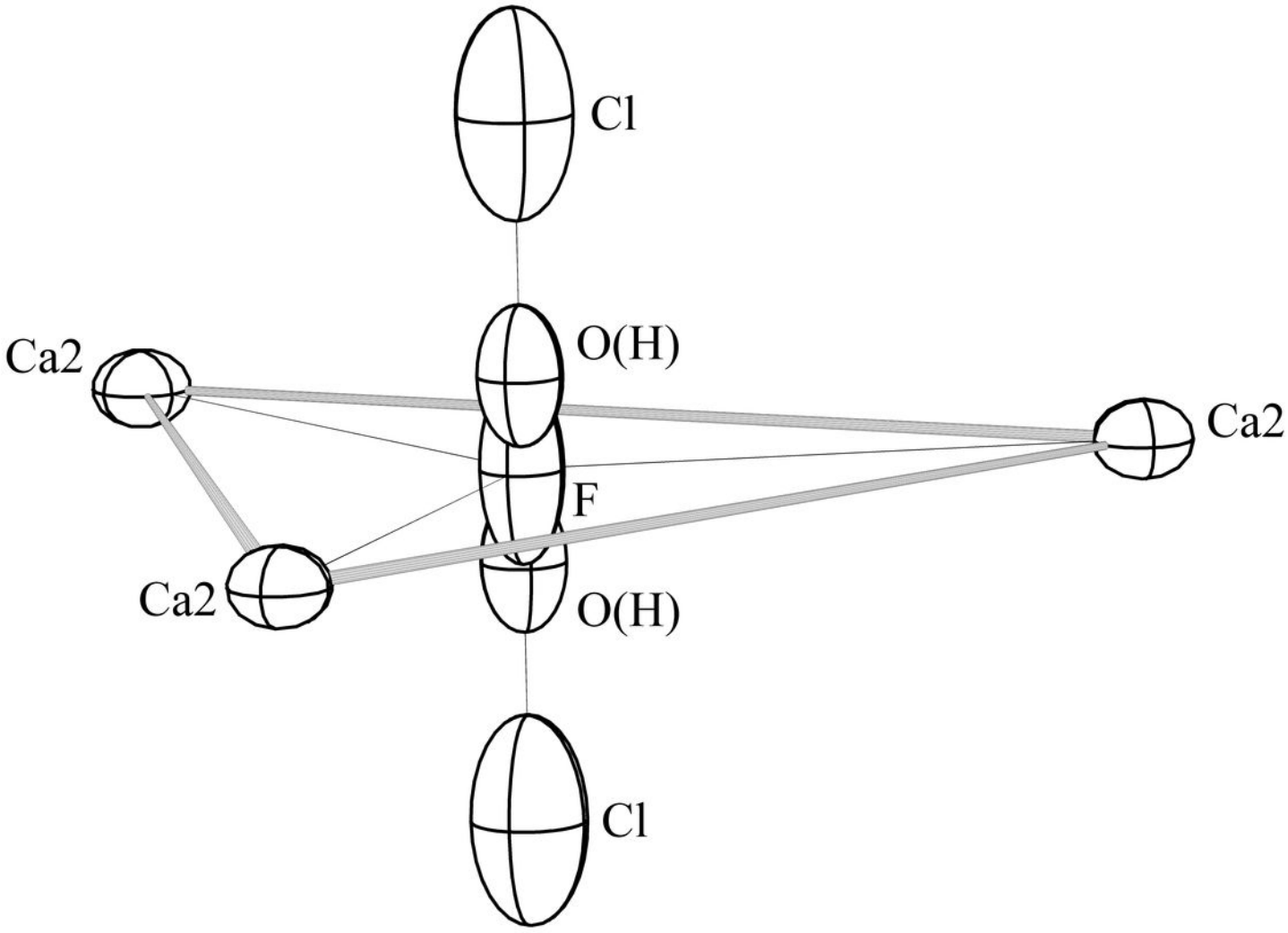
Cl
O(H)
Ca2
Ca2
F
Ca2
O(H)
Cl

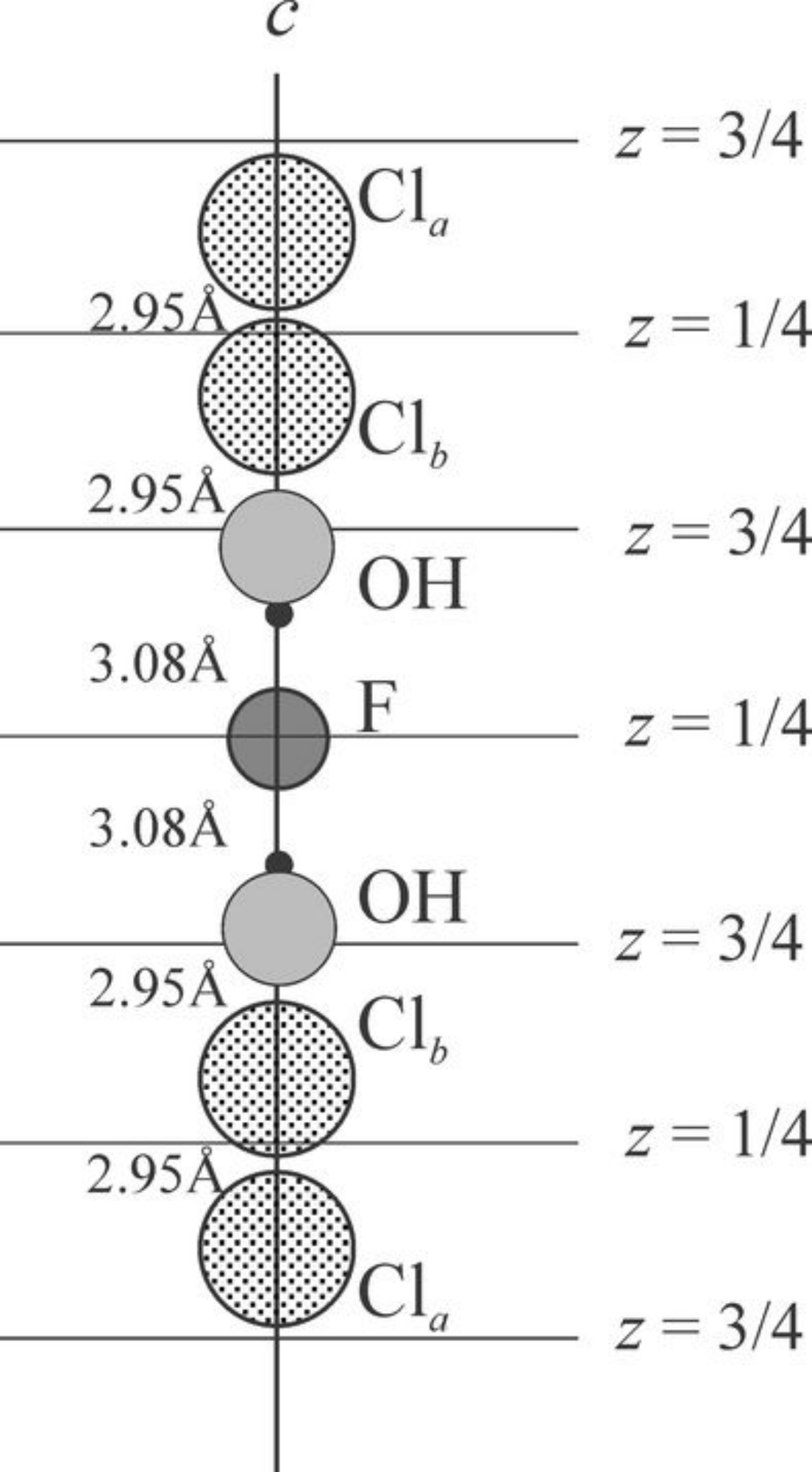
c
z = 3/4
Cl$_a$
2.95Å
z = 1/4
Cl$_b$
2.95Å
z = 3/4
OH
3.08Å
F
z = 1/4
3.08Å
OH
z = 3/4
2.95Å
Cl$_b$
z = 1/4
2.95Å
Cl$_a$
z = 3/4

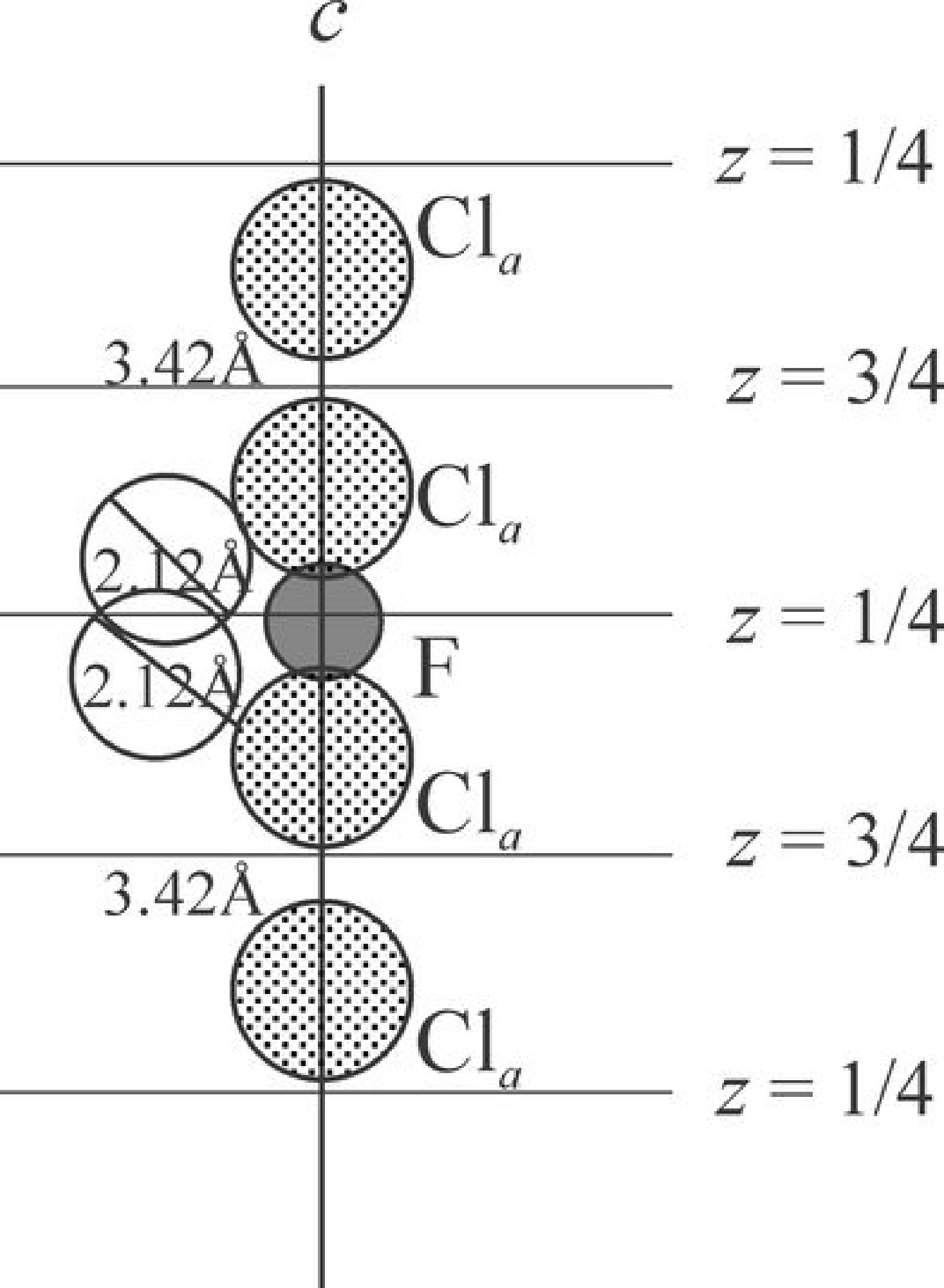
c
z = 1/4
Cl$_a$
3.42Å
z = 3/4
Cl$_a$
2.12Å
z = 1/4
F
2.12Å
Cl$_a$
z = 3/4
3.42Å
Cl$_a$
z = 1/4

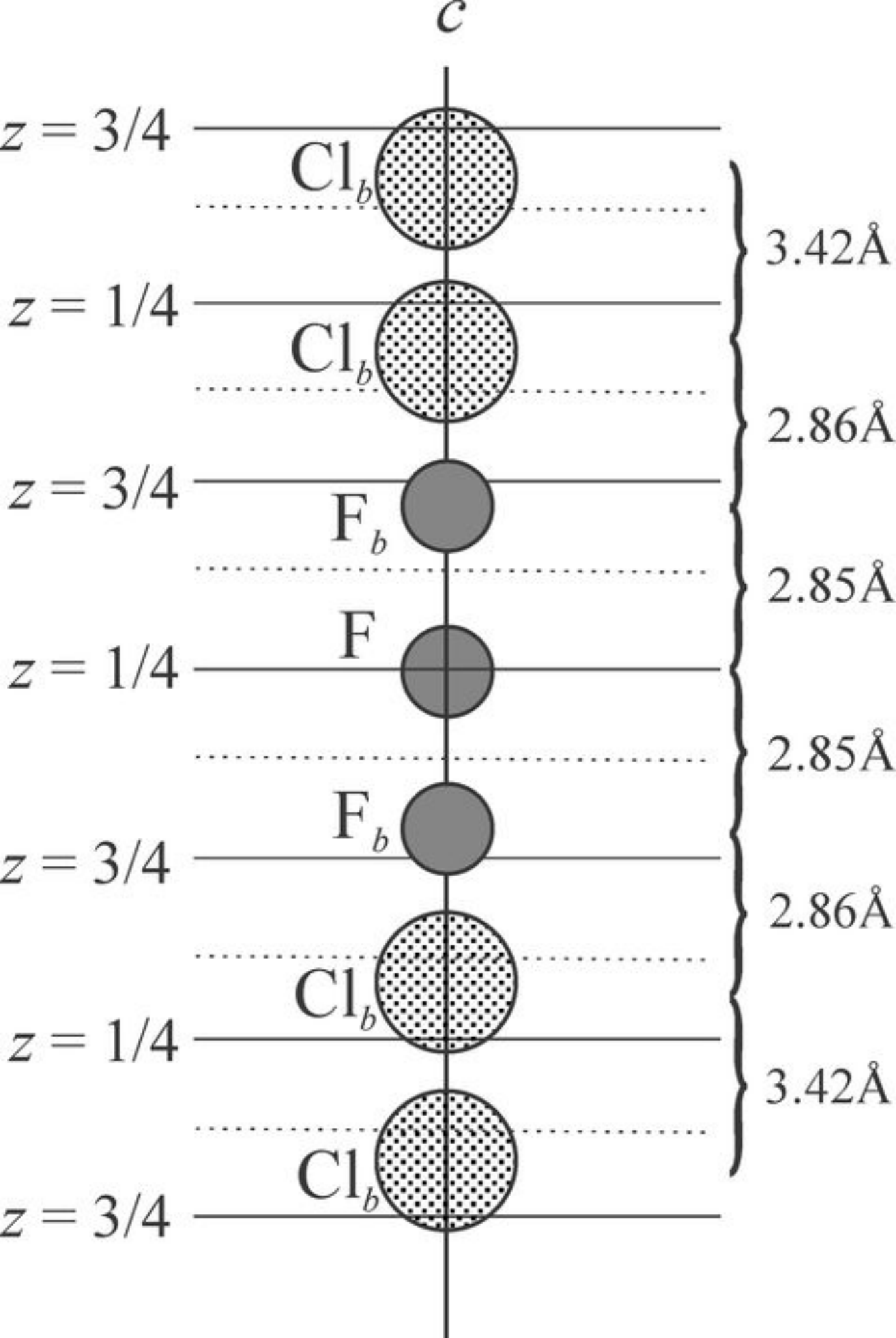
c
z = 3/4
Cl$_b$
3.42Å
z = 1/4
Cl$_b$
2.86Å
z = 3/4
F$_b$
2.85Å
F
z = 1/4
2.85Å
F$_b$
z = 3/4
2.86Å
Cl$_b$
z = 1/4
3.42Å
Cl$_b$
z = 3/4

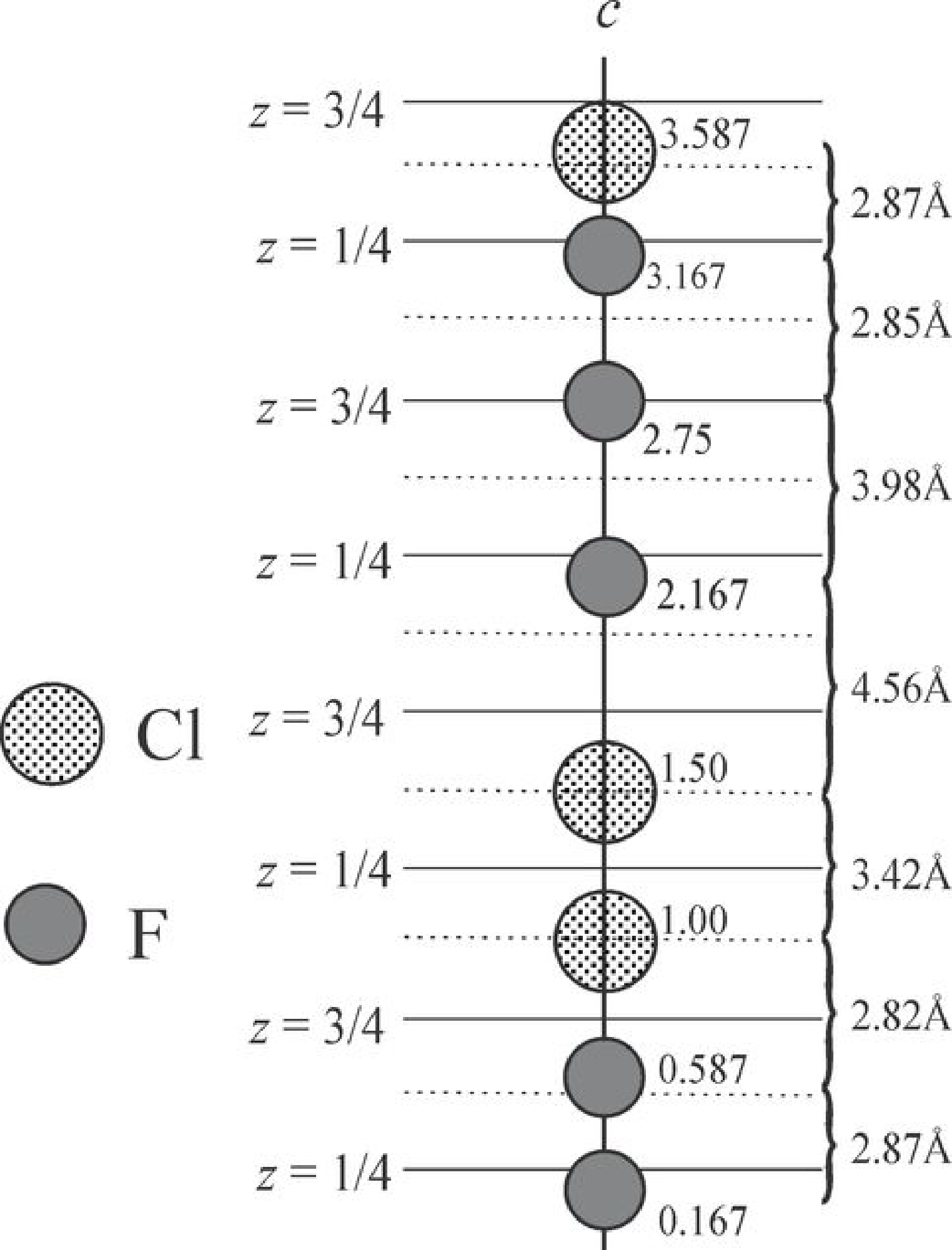
c
z = 3/4
3.587
2.87Å
z = 1/4
3.167
2.85Å
z = 3/4
2.75
3.98Å
z = 1/4
2.167
4.56Å
z = 3/4
1.50
z = 1/4
3.42Å
1.00
z = 3/4
2.82Å
0.587
z = 1/4
2.87Å
0.167
Cl
F